eLIFE elifesciences.org

RESEARCH ARTICLE

Figures and figure supplements

Multivalency of NDC80 in the outer kinetochore is essential to track shortening microtubules and generate forces

Vladimir A Volkov *et al*

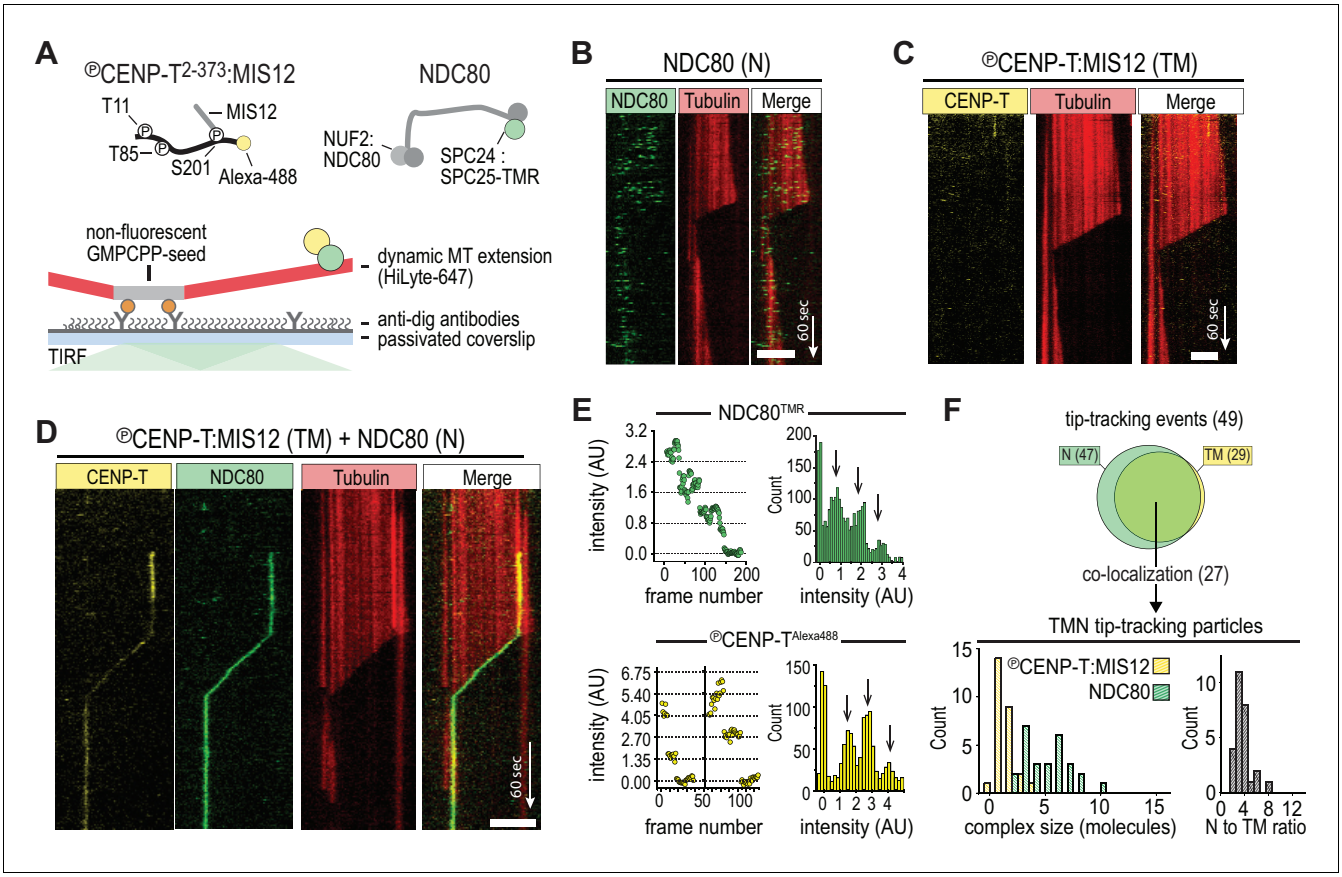

Figure 1. CENP-T-mediated oligomerization of NDC80 produces particles that follow microtubule disassembly. (**a**) Schematic representation of Alexa-488-labeled, phosphorylated CENP-T:MIS12 and TMR-labeled NDC80 in a single-molecule TIRF setup with dynamic microtubules. (**b**) Monomeric NDC80 at 200 pM does not follow microtubule shortening. (**c**) MIS12-CENP-T at 2 nM does not bind to microtubules and does not follow microtubule shortening. (**d**) MIS12:CENP-T^{Alexa488} (2 nM, yellow) and NDC80^{TMR} (20 pM, green) mixed in the flow-chamber, co-localize in a particle that follows the shortening end of a microtubule. (**e**) Left: time traces showing photobleaching of NDC80^{TMR} (green) and CENP-T^{Alexa488} particles (yellow). Note that the CENP-T particle initially bleaches two fluorophores simultaneously. Right: distributions containing all bleaching traces (n = 13 for TMR and n = 20 for Alexa488). Arrows show intensities of 1, 2 and 3 fluorophores. See Materials and methods for details. (**f**) Euler diagram of tip-tracking particles produced by mixing NDC80 and MIS12:CENP-T (top). Distributions of initial, unbleached fluorescence intensities (expressed as the number of fluorophores) of NDC80^{TMR} (green) and MIS12:CENP-T^{Alexa488} (yellow) in the tip-tracking particles containing both signals (bottom left). Black bars show ratio of NDC80 to CENP-T (bottom right). Scale bars: 5 μm (horizontal), 60 s (vertical).

DOI: https://doi.org/10.7554/eLife.36764.003

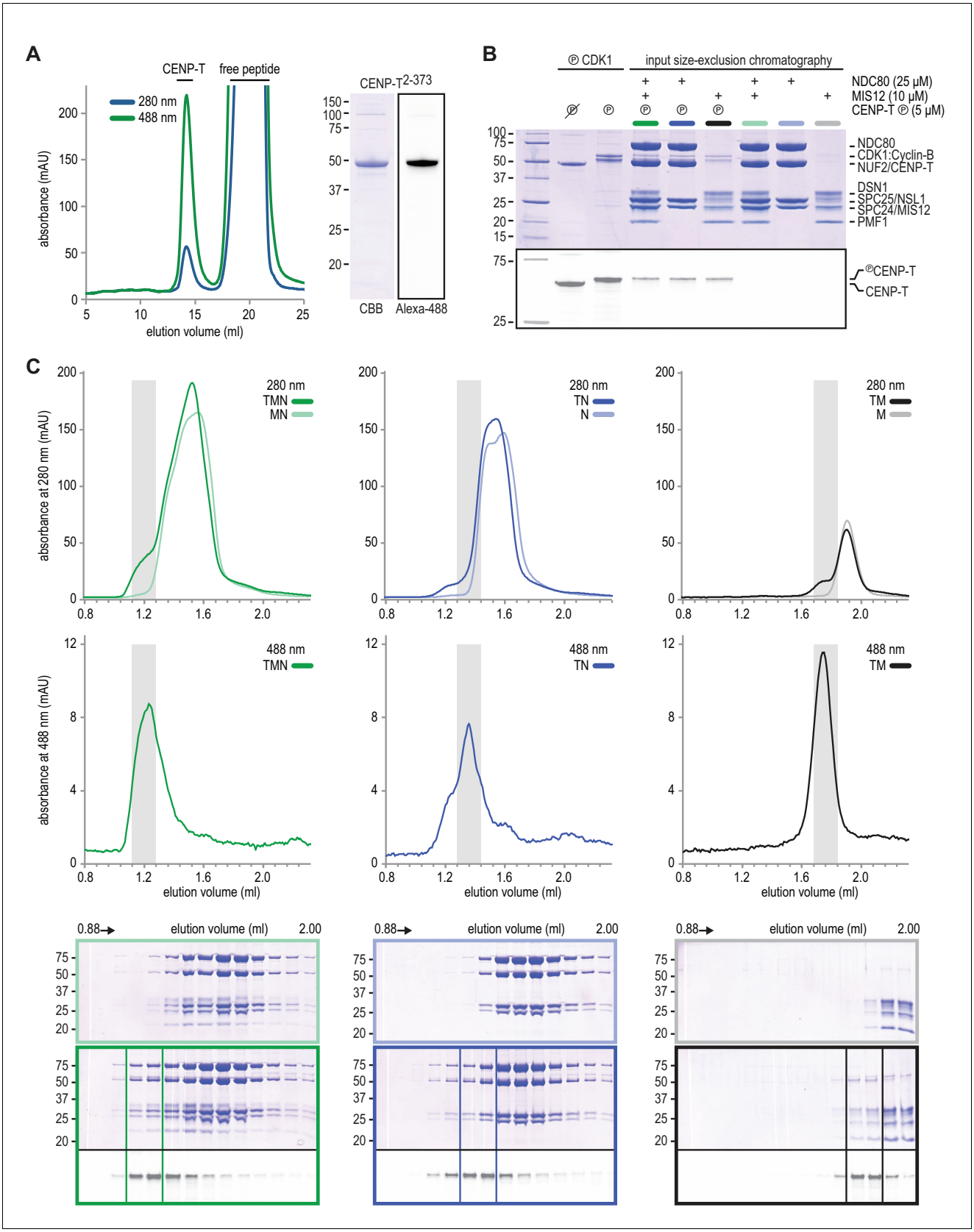

Figure 1—figure supplement 1. Reconstitution of NDC80 and MIS12 on CENP-TAlexa-488 phosphorylated by CDK1:Cyclin-B. (**a**) CENP-T$^{2-373}$ labelled with Alexa-488 was separated from the excess of GGGGC-Alexa488 peptide by size-exclusion chromatography. (**b**) SDS-PAGE analysis to demonstrate

Figure 1—figure supplement 1 continued on next page

Figure 1—figure supplement 1 continued

the phosphorylation of CENP-T by CDK1:Cyclin-B and to compare the input for size-exclusion chromatography shown in panel C. (**c**) MIS12 and NDC80 bind phosphorylated CENP-T. Size-exclusion chromatography traces (top) and SDS-PAGE analysis (bottom) of TMN (green), TN (blue) and TM (black). The two shaded fractions were pooled for single-molecule TIRF experiments.

DOI: https://doi.org/10.7554/eLife.36764.004

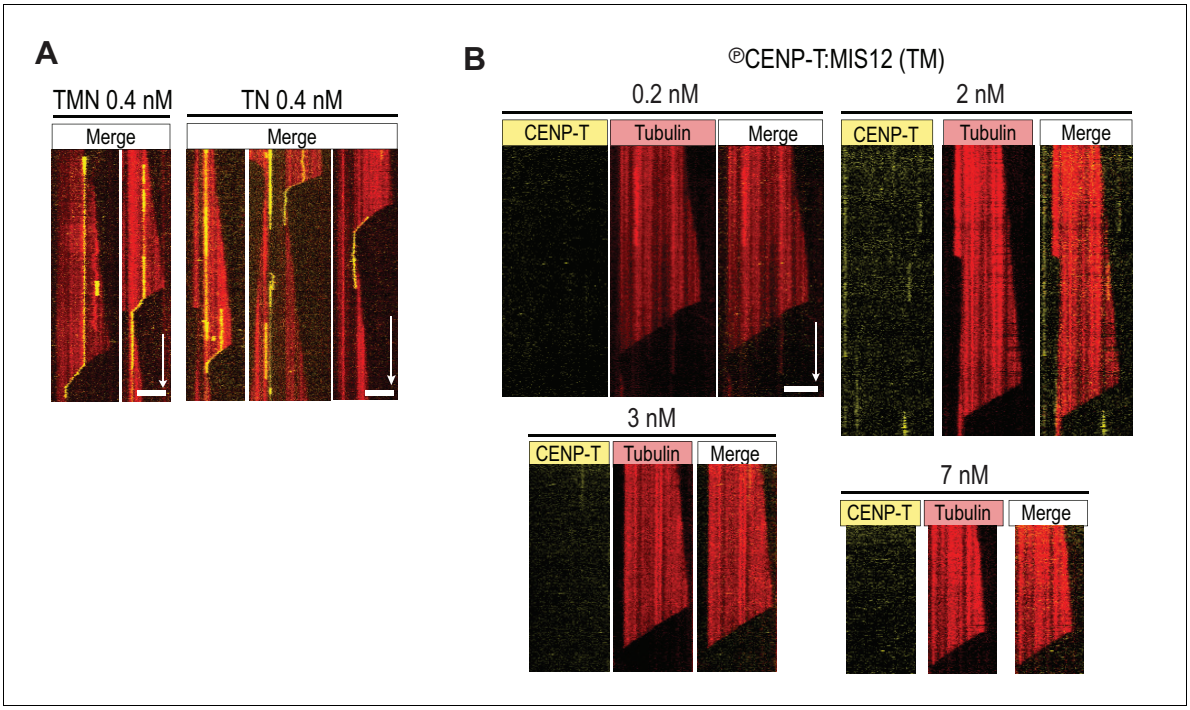

Figure 1—figure supplement 2. NDC80 promotes tip-tracking of reconstituted TN and TMN. (**a**) TMN and TN (both at 0.4 nM) follow shortening microtubules in a single-molecule TIRF experiment. (**b**) TM does not bind to microtubules and does not follow microtubule shortening in a concentration range from 0.2 to 7 nM. Scale bars: 5 μm (horizontal), 60 s (vertical).

DOI: https://doi.org/10.7554/eLife.36764.005

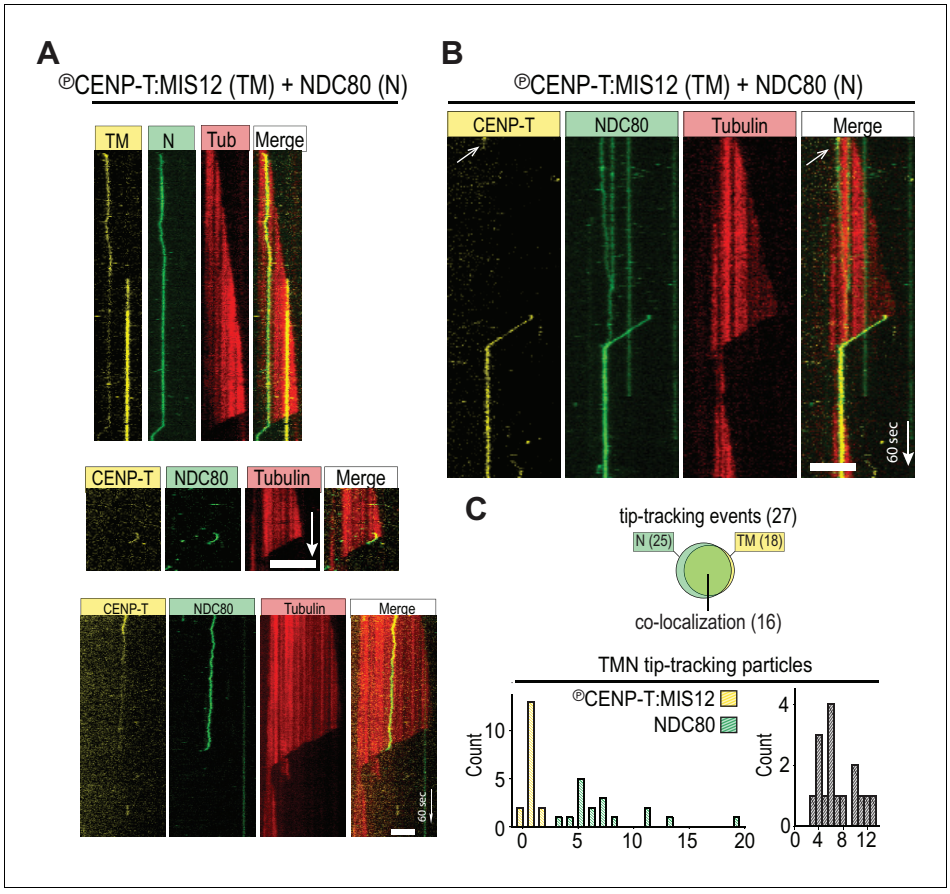

Figure 1—figure supplement 3. Tip-tracking by NDC80 oligomerized on CENP-T:MIS12. (**a**) Two example kymographs as in ***Figure 1D***. (**b**) Example kymograph of co-localizing $NDC80^{TMR}$ and $CENP\text{-}T^{Alexa488}$:MIS12 on the microtubule lattice and at the shortening microtubule end in a flow chamber with a 1:1 N/TM (both added at 200 pM). The white arrow indicates a CENP-T bleaching event. (**c**) Quantification of tip-tracking events as in ***Figure 1F*** for particles containing initially both TMR and Alxa488 signal at 200 pM of both $NDC80^{TMR}$ and $CENP\text{-}T^{Alexa488}$:MIS12. 5 μm (horizontal), 60 s (vertical).

DOI: https://doi.org/10.7554/eLife.36764.006

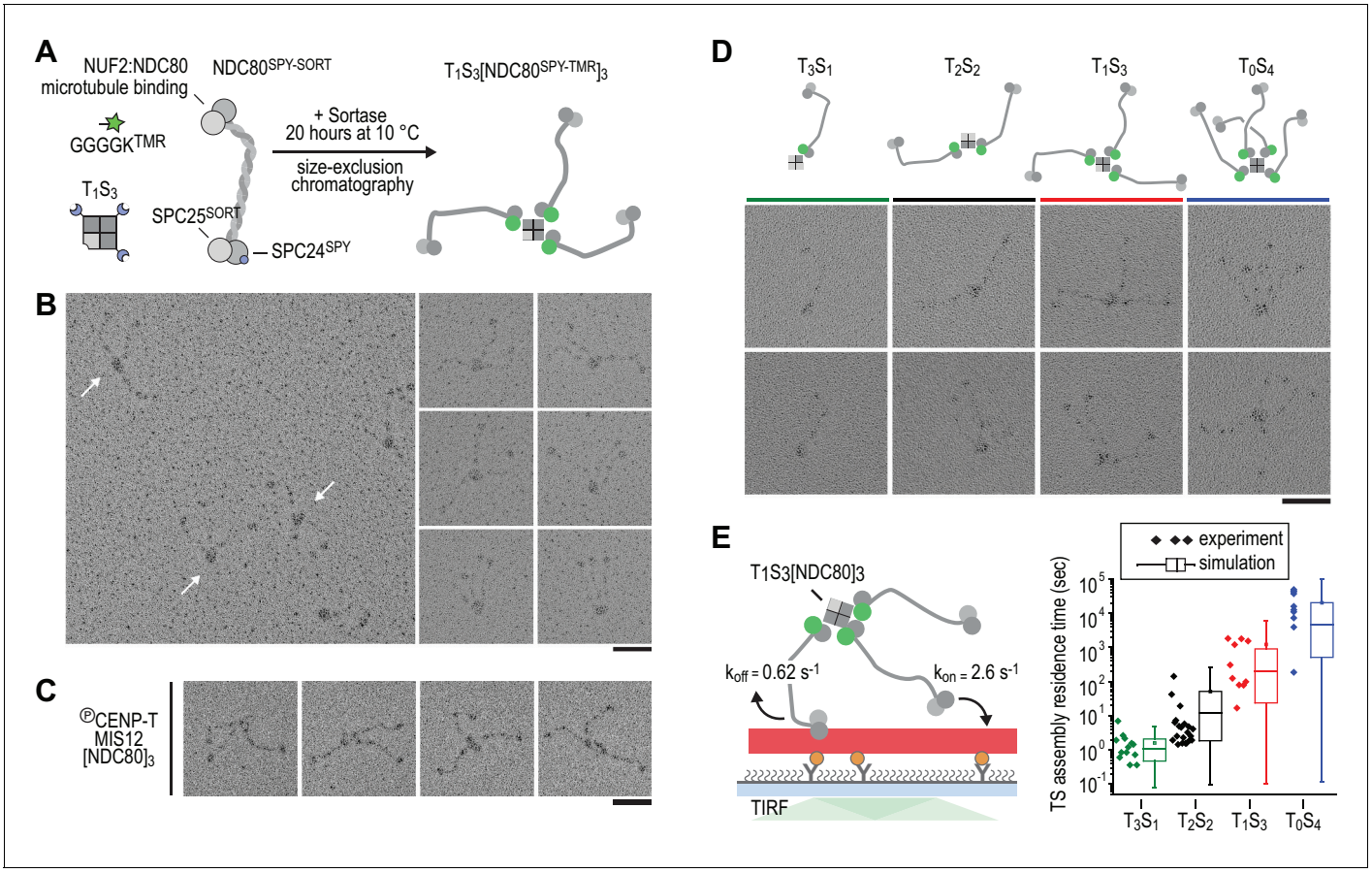

Figure 2. Incremental addition of NDC80 results in hyperstable microtubule binding. (**a**) NDC80$^{SPY\text{-}SORT}$ was fluorescently labelled and covalently bound to TS assemblies. The cartoon shows the formation of $T_1S_3[NDC80]_3$ assemblies. Size-exclusion chromatography and SDS-PAGE analysis are shown in ***Figure 1—figure supplement 1***. (**b**) $T_1S_3[NDC80]_3$ assemblies were analysed by electron microscopy after low-angle rotary shadowing. Three flexible NDC80 complexes of approximately 60 nm originate from central T_1S_3 densities (white arrows in the field of view) Scale bar 50 nm. (**c**) Representative micrographs of CENP-T:MIS12:$[NDC80]_3$ as analysed previously (***Huis In 't Veld et al., 2016***). (**d**) Side-by-side comparison of NDC80 coupled to T_3S_1, T_2S_2, T_1S_3, and T_0S_4. Cartoons represent the approximate orientation of assemblies in the upper row of micrographs. Scale bar 50 nm. (**e**) Residence time of quantized NDC80 assemblies on taxol-stabilized microtubules as determined experimentally (dots) and as predicted by a series of 1000 simulations (box and whiskers plot; box: 25–75%, horizontal line: median, whiskers: 5–95%). NDC80 complexes of a microtubule-bound TS-NDC80 assembly attach to and detach from microtubules with rates of k_{on} and k_{off}, respectively. The residence time of an oligomer is defined as the time between the association of its first NDC80 tether and the detachment of all NDC80 tethers.

DOI: https://doi.org/10.7554/eLife.36764.007

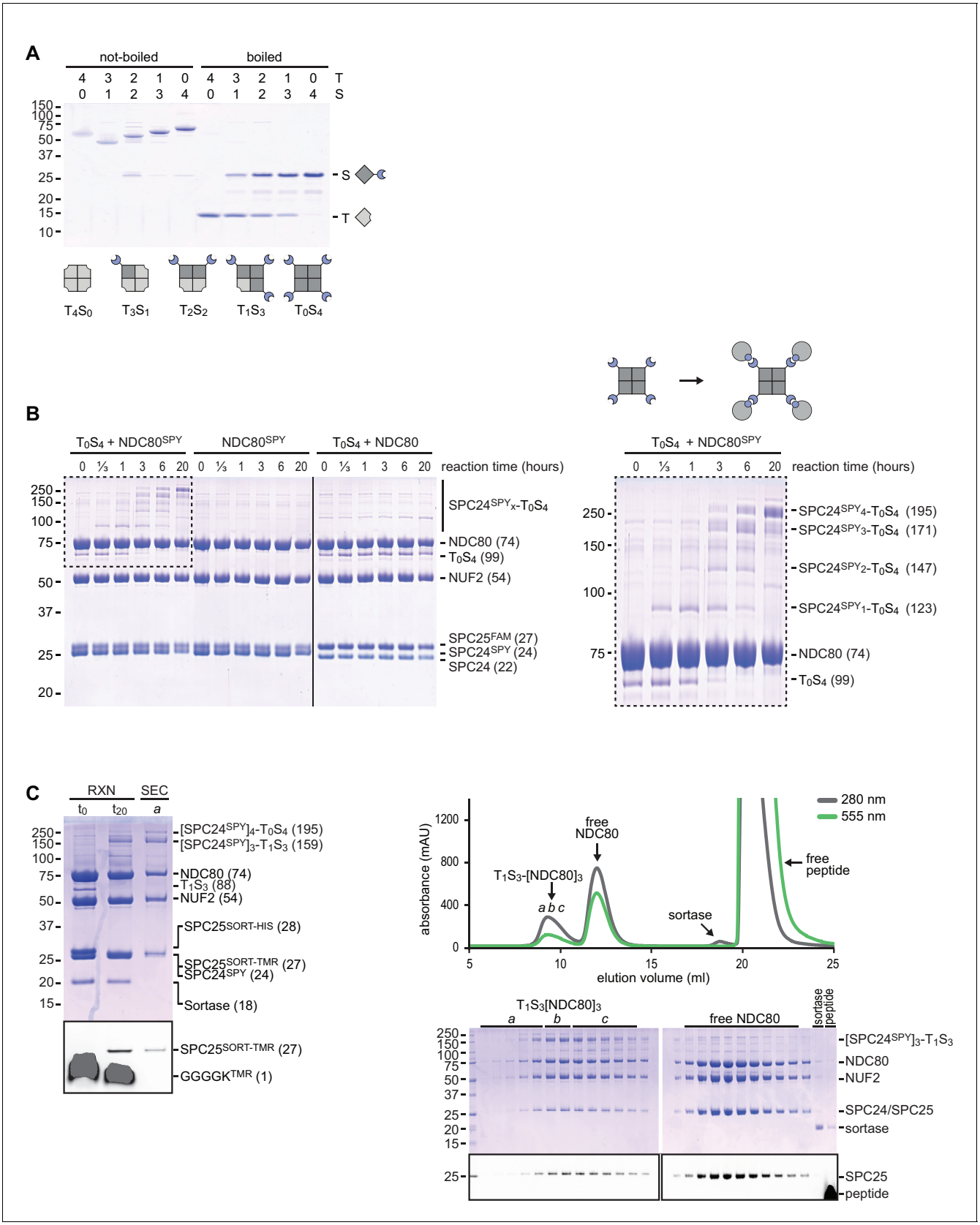

Figure 2—figure supplement 1. A reconstituted system to precisely control NDC80 stoichiometry (Part I). (**a**) T_yS_x variants were separated by ion-exchange chromatography based on the pI difference of T (5.1) and S (4.5). Collected assemblies were analyzed by SDS-PAGE as tetramers (not-boiled)

Figure 2—figure supplement 1 continued on next page

Figure 2—figure supplement 1 continued

or in a denatured form (boiled). (**b**) SDS-PAGE analysis (samples not-boiled) to monitor the formation of S-SPC24^{SPY} complexes. NDC80 complexes without added T_0S_4 or without a SPY-tag were analysed as a control. The boxed area is shown at larger magnification on the right. (**c**) Samples before (t_0) and after (t_{20}) the reaction were analysed by SDS-PAGE (samples not-boiled) to monitor coupling of SPC24^{SPY} to T_1S_3 tetramers and fluorescent labelling of SPC25^{SORT}. Size-exclusion chromatography was used to separate T_1S_3[NDC80]$_3$ assemblies from sortase and from the excess of unreacted NDC80 and free peptide. The lower panels show the GGGGK^{TMR} and SPC25^{TMR} in-gel fluorescence.

DOI: https://doi.org/10.7554/eLife.36764.008

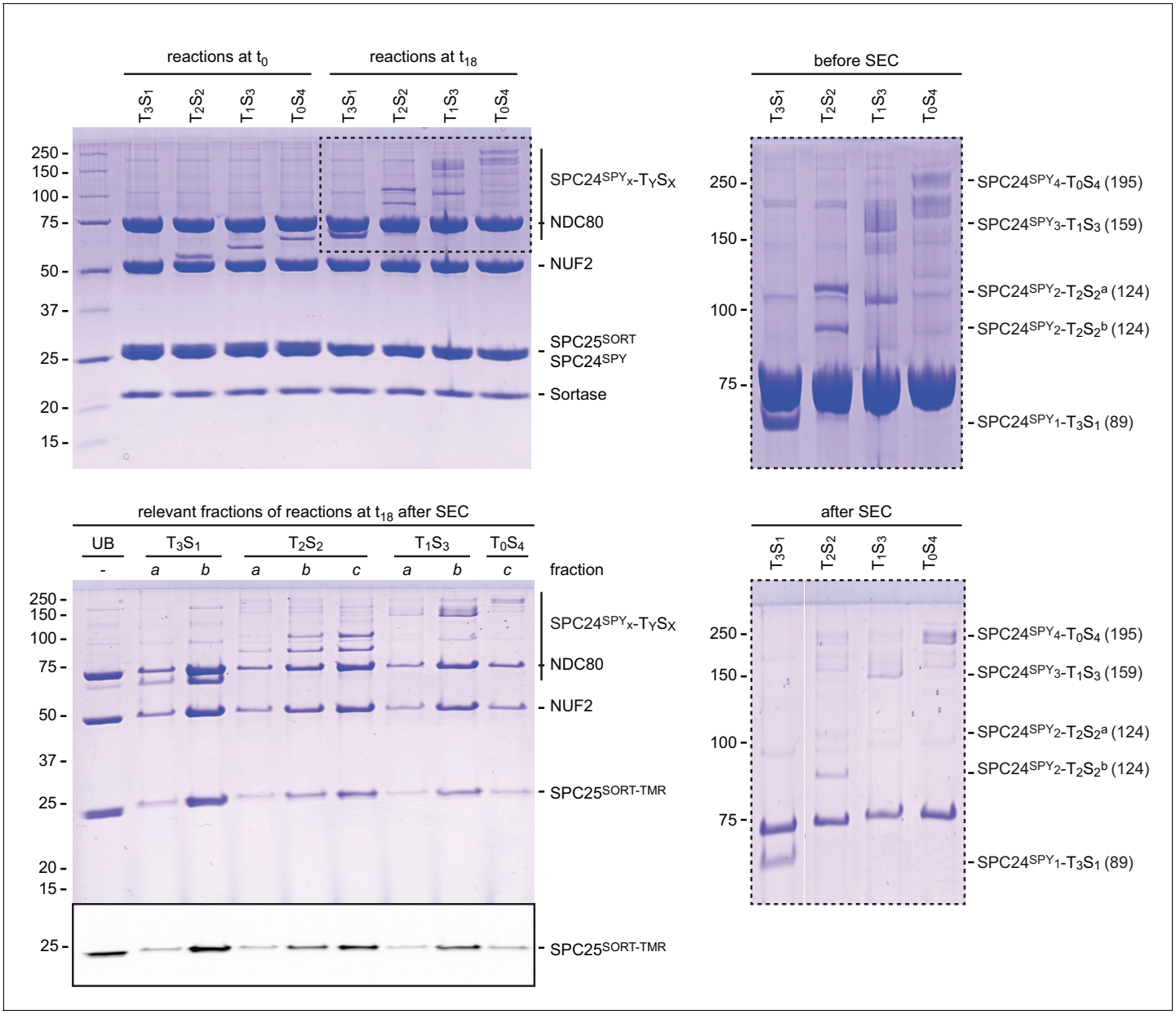

Figure 2—figure supplement 2. A reconstituted system to precisely control NDC80 stoichiometry (Part II). Samples before (t_0) and after (t_{18}) the reaction were analysed by SDS-PAGE (samples not-boiled) to monitor coupling of $SPC24^{SPY}$ to T_yS_x tetramers and fluorescent labelling of $SPC25^{SORT}$. Size-exclusion chromatography was used to separate $T_yS_x[NDC80]_x$ assemblies from sortase and from the excess of unreacted NDC80 and free peptide. Fractions *a*, *b*, and *c*, indicate the front, middle, and tail of the peak as in panel C.

DOI: https://doi.org/10.7554/eLife.36764.009

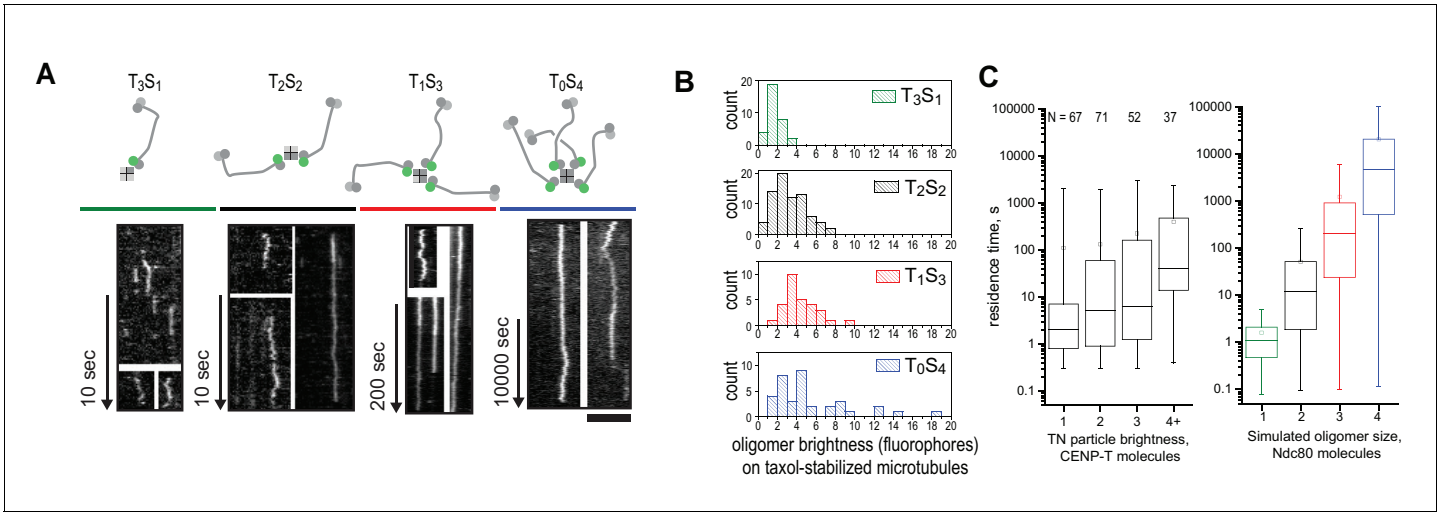

Figure 2—figure supplement 3. Characterization of oligomerized NDC80 on taxol-stabilized microtubules. (**a**) Kymographs of mono-, di-, tri-, and tetravalent NDC80 complexes binding to taxol stabilized microtubules. Scale bar 5 μm. (**b**) Brightness distribution of TS-NDC80 assemblies on taxol-stabilized microtubules. (**c**) Residence time of co-purified CENP-T:NDC80 on taxol-stabilized microtubules, grouped by initial intensity of CENP-T^{Alexa488} fluorescence (left). Box: 25–75%, whiskers: min-max. Right: residence time of simulated NDC80 monomers, dimers, trimers and tetramers (see also ***Figure 2E***). Box: 25–75%, whiskers: 5–95%.

DOI: https://doi.org/10.7554/eLife.36764.010

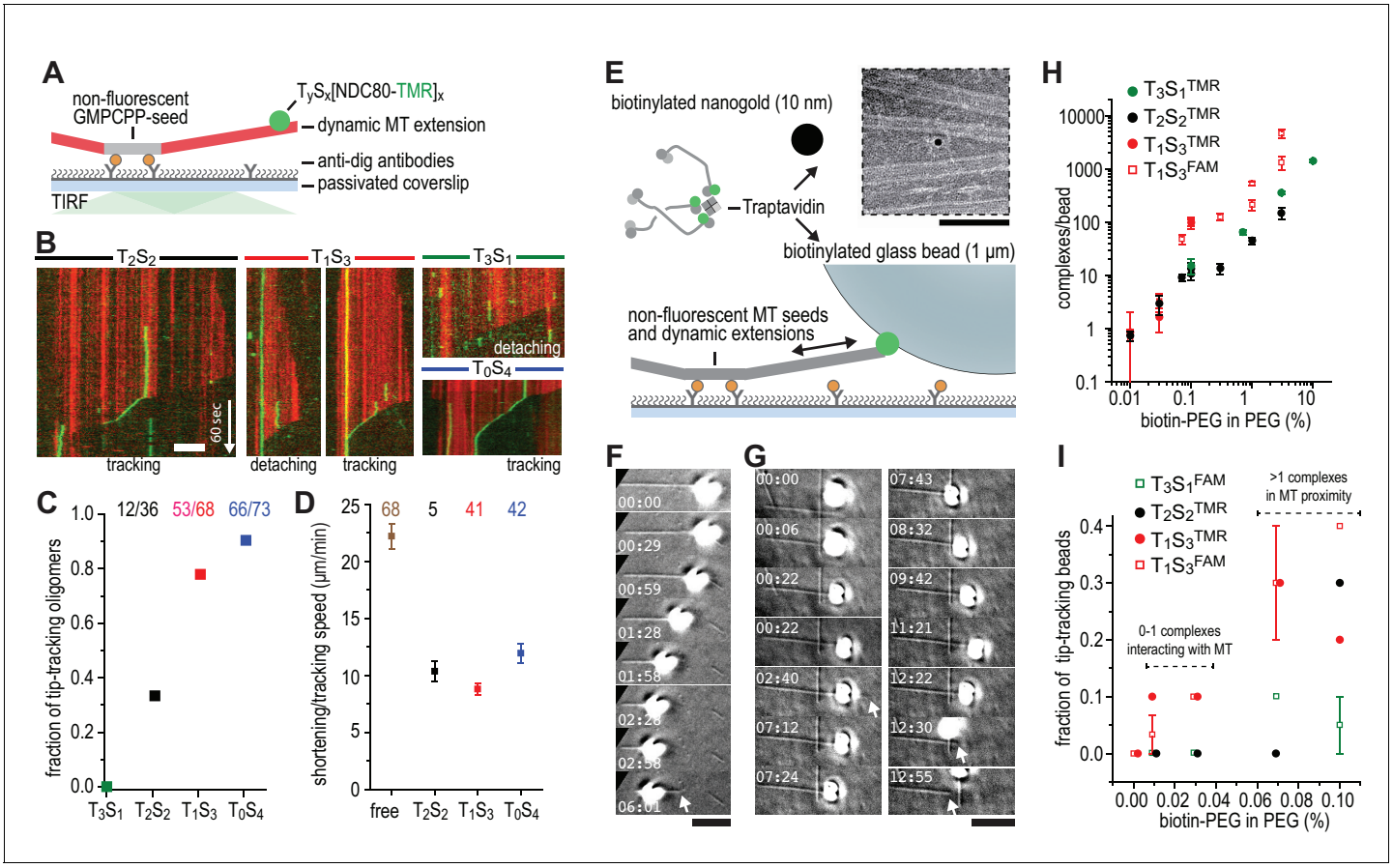

Figure 3. Trivalent TS-NDC80 efficiently tracks depolymerizing microtubules and transports cargo. (**a**) Schematic representation of the experimental setup. (**b**) Kymographs showing NDC80 (green) assembled on T_2S_2, T_1S_3, or T_0S_4 tracking a depolymerizing microtubule (red). An example of a T_1S_3[NDC80]$_3$ complex that detached from the tip of shortening microtubule is also included. Scale bar 5 μm. See ***Figure 3—figure supplement 1*** and ***Video 1***. (**c**) The fraction of NDC80 assemblies that track depolymerizing microtubules. (**d**) Comparison between microtubule depolymerization in the presence and absence of TS-NDC80 following the shortening tips. Data are shown as mean ± SEM. **e**) Biotinylated glass beads or nanogold particles can be conjugated to traptavidin in TS-NDC80C assemblies. Nanogold particles coated with T_1S_3[NDC80]$_3$ bound to microtubules as observed by negative-staining EM (see also ***Figure 3—figure supplement 2***). Scale bar 100 nm. (**f–g**) Examples of glass beads coated with T_1S_3[NDC80]$_3$ tracking depolymerizing microtubules. The bead in panel g follows the growing microtubule after a rescue event until it detaches during a second depolymerization phase. White arrows indicate the dynamic microtubule tips. Scale bar 5 μm. (**h**) Fluorescence-based quantification of the number of complexes on glass beads coated with increasing amounts of PLL-PEG-biotin. (**i**) The fraction of beads coated with various TS-NDC80 assemblies that track depolymerizing microtubules as a function of the amount of biotin-PEG added to the beads.

DOI: https://doi.org/10.7554/eLife.36764.011

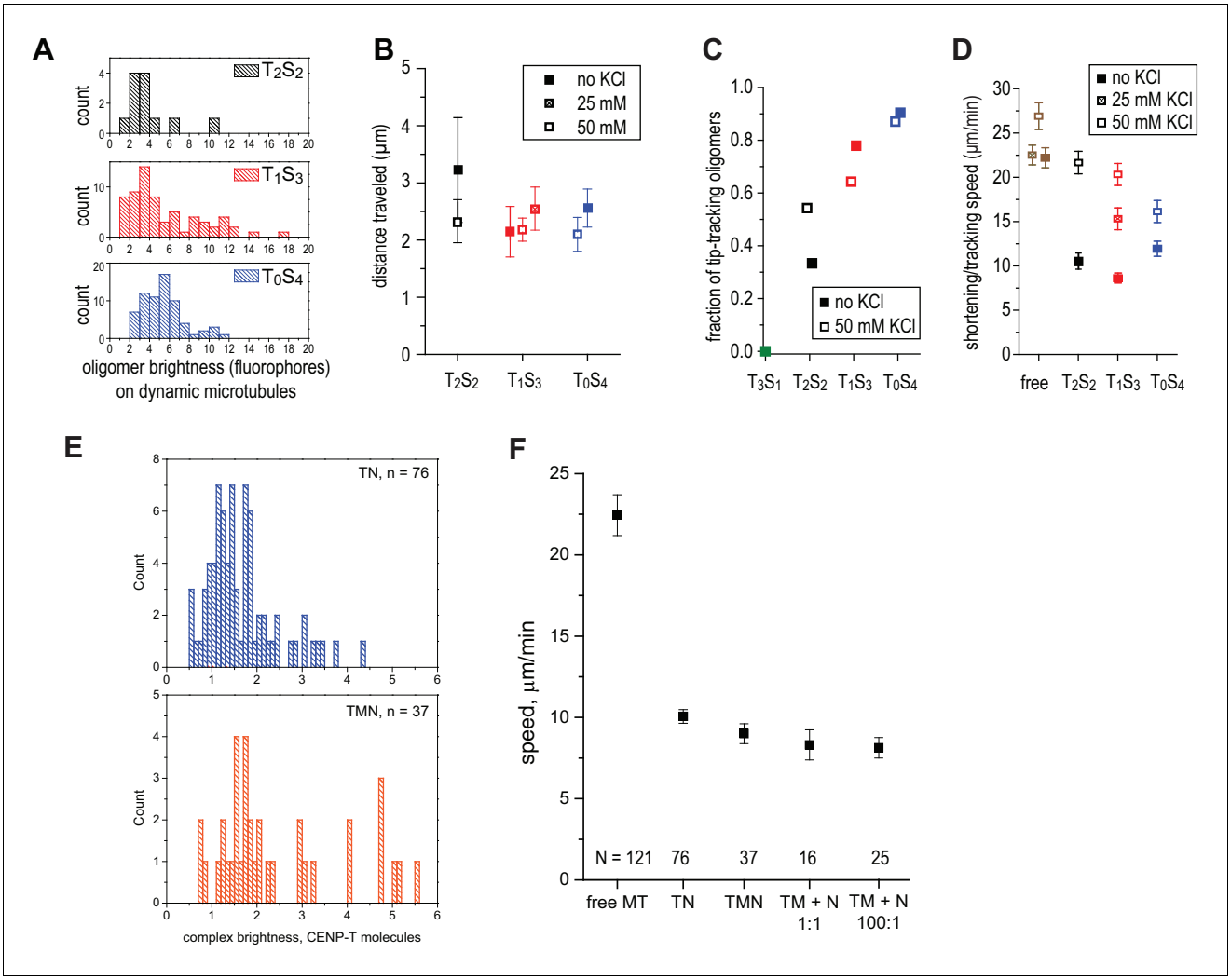

Figure 3—figure supplement 1. Characterization of oligomerized NDC80 on dynamic microtubules. (**a**) Brightness distribution of TS-NDC80 assemblies on dynamic microtubules. **b**) Distance travelled by TS-NDC80 modules moving with the tips of the shortening microtubules. (**c–d**) Presence of 25–50 mM KCl in the motility buffer does not prevent TS-NDC80 assemblies from tip-tracking and slowing down the microtubule shortening. (**e**) Histograms of initial intensities of TN and TMN spots following the shortening ends of the microtubules. (**f**) Pre-assembled TN and TMN, as well as TM mixed with N in the flow-chamber, slow down microtubule shortening (left, see also ***Figure 1D,F***) to the same extent as TS-NDC80 modules (see also ***Figure 3B,D***). Data are shown as mean ± SEM.

DOI: https://doi.org/10.7554/eLife.36764.012

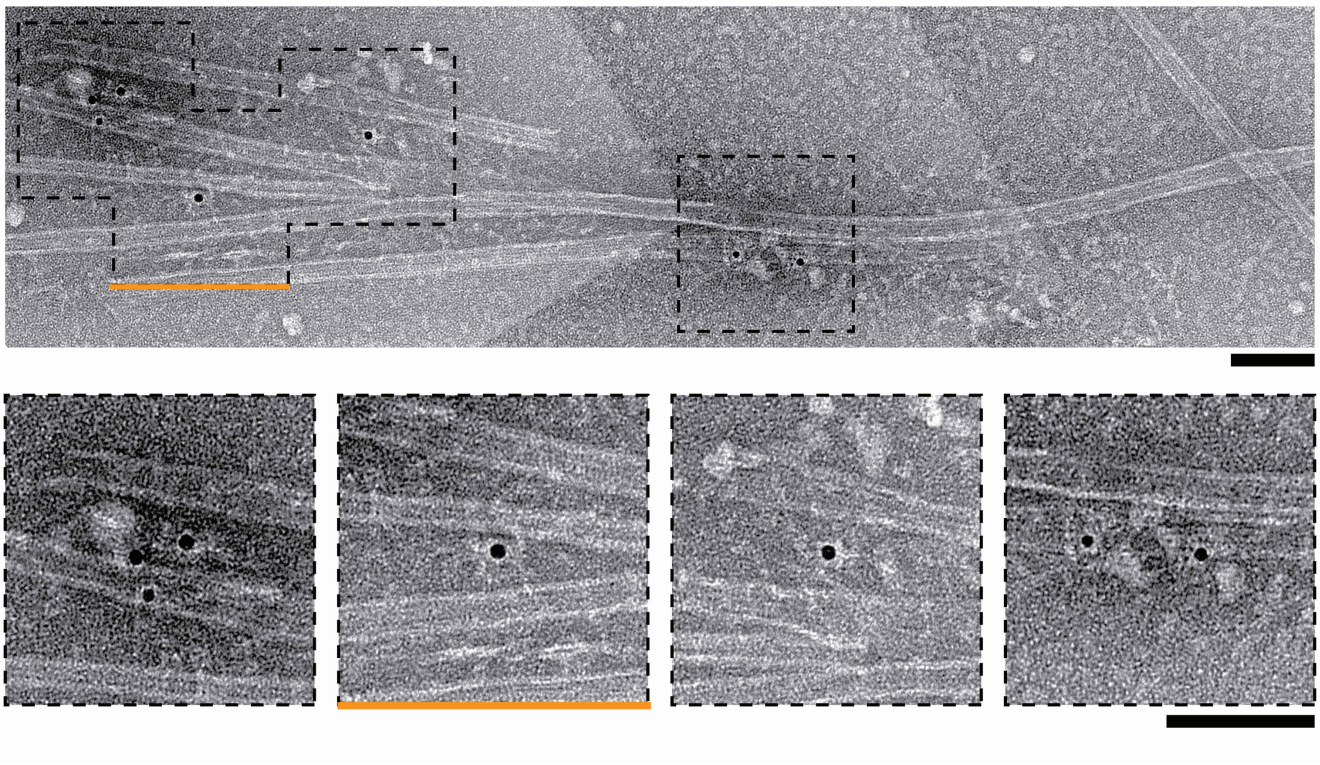

Figure 3—figure supplement 2. Negative-stain EM of microtubules and nanogold particles coated with $T_1S_3[NDC80]_3$. Boxed areas in the upper micrograph are shown below at a higher magnification. The orange line marks the micrograph shown in main ***Figure 2E***. Scale bars 100 nm.
DOI: https://doi.org/10.7554/eLife.36764.013

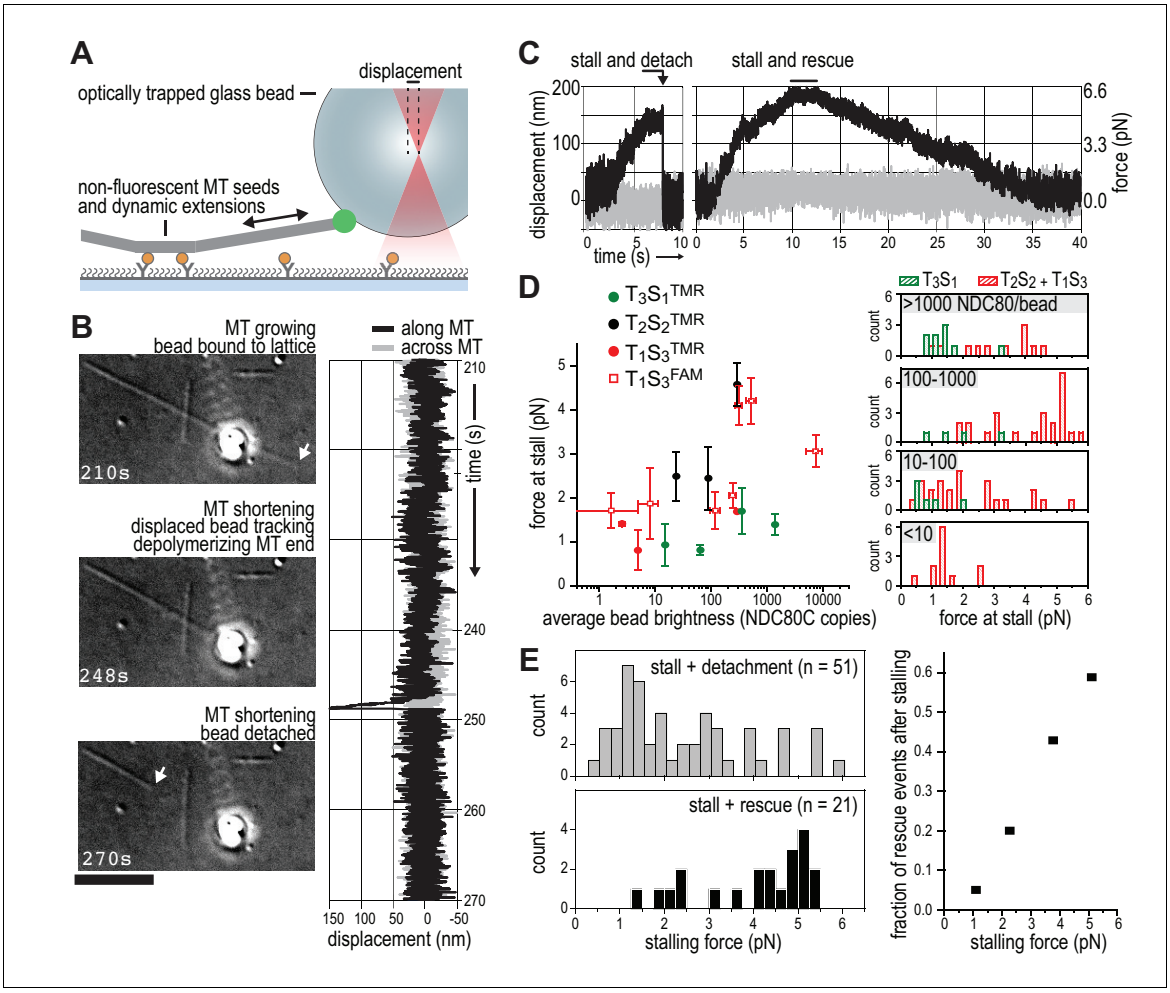

Figure 4. TS-NDC80 modules stall and rescue microtubule depolymerization. (**a**) The displacement of an optically trapped glass bead can be used to determine the force exerted by a shortening microtubule on a bead-bound TS-NDC80 oligomer. (**b**) Example of a trapped glass bead that is displaced along the microtubule axis as it holds on to a depolymerizing microtubule (248 s). Arrows point to the dynamic microtubule tip before (210 s) and after (270 s) the force development. The graph on the right shows unfiltered QPD signal along and across the microtubule axis. (**c**) Examples of unfiltered QPD signals recorded during microtubule shortening. Stalling of microtubule depolymerization by the coupled bead in the optical trap is followed by detachment of the bead (left) or a rescue of microtubule growth (right). (**d**) Average forces at which differently coated beads stall shortening microtubules. Data are shown as mean ±SEM. (**e**) Distribution of stalling forces that were followed by bead detachment from the microtubule (grey bars) or microtubule rescue (black bars). These distributions were used to calculate the fraction of events leading to a force-induced rescue (right).
DOI: https://doi.org/10.7554/eLife.36764.016

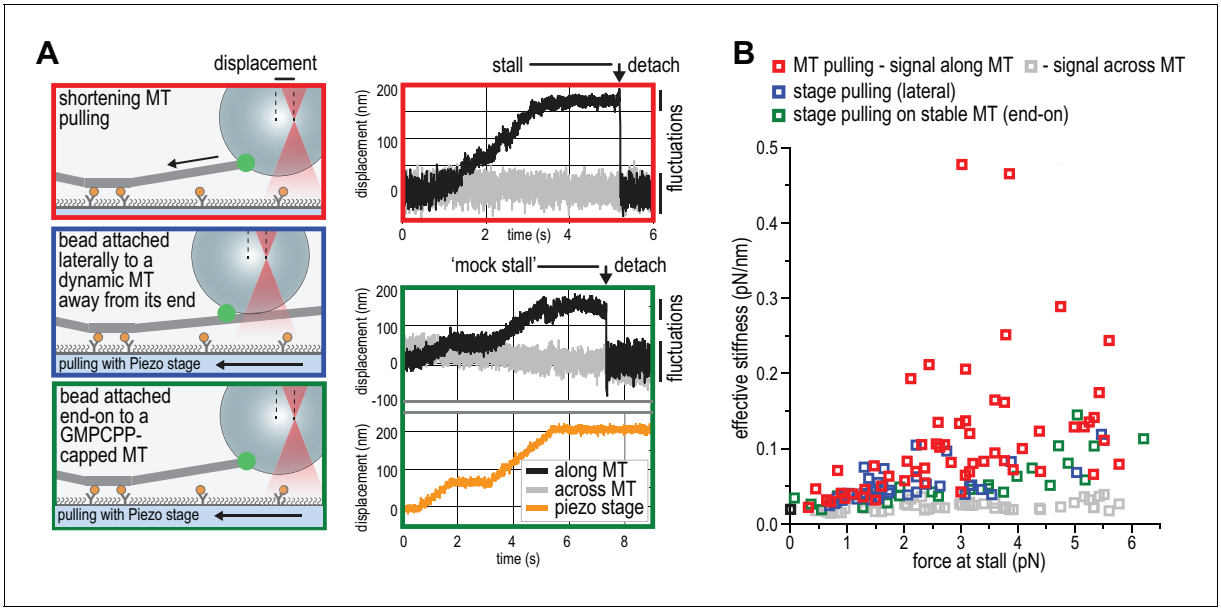

Figure 5. NDC80C oligomers stall microtubules through interaction with the shortening microtubule end. (**a**) Experimental setup to compare forces generated by shortening microtubules (red box) with forces generating by a moving stage while a bead with $T_1S_3[NDC80]_3$ is attached laterally to a dynamic microtubule (blue box), or end-on to a stabilized microtubule (green box). Examples of unfiltered QPD signals recorded during force generation are shown on the right. (**b**) Effective stiffness of the link between the bead and the microtubule increases with force.

DOI: https://doi.org/10.7554/eLife.36764.019

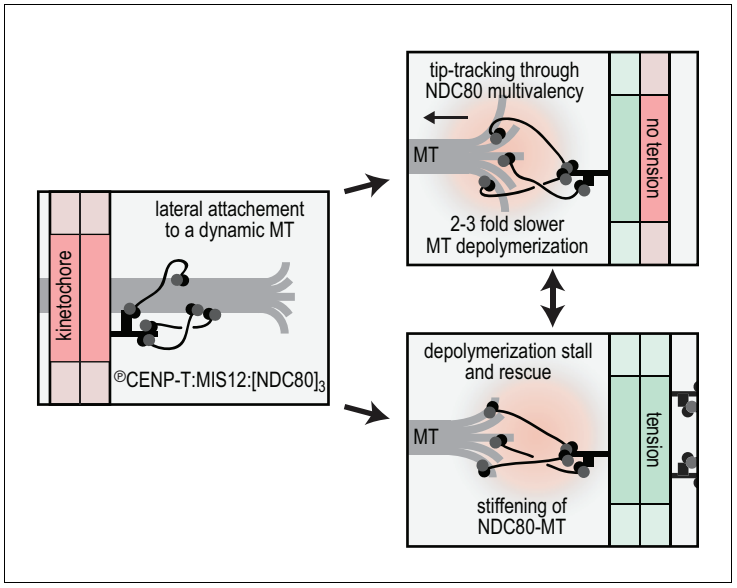

Figure 6. Reconstitution of a dynamic kinetochore-microtubule attachment. A graphical recapitulation of the kinetochore-microtubule interfaces reconstituted and characterised in this study and their occurrence in vivo.
DOI: https://doi.org/10.7554/eLife.36764.020